J Transp Secur (2011) 4:73–94
DOI 10.1007/s12198-010-0059-7

An evaluation of airport x-ray backscatter units based on image characteristics

Leon Kaufman · Joseph W. Carlson

Received: 27 October 2010 / Accepted: 9 November 2010 / Published online: 26 November 2010

Abstract Little information exists on the performance of x-ray backscatter machines now being deployed through UK, US and other airports. We implement a Monte Carlo simulation using as input what is known about the x-ray spectra used for imaging, device specifications and available images to estimate penetration and exposure to the body from the x-ray beam, and sensitivity to dangerous contraband materials. We show that the body is exposed throughout to the incident x-rays, and that although images can be made at the exposure levels claimed (under 100 nanoGrey per view), detection of contraband can be foiled in these systems. Because front and back views are obtained, low Z materials can only be reliable detected if they are packed outside the sides of the body or with hard edges, while high Z materials are well seen when placed in front or back of the body, but not to the sides. Even if exposure were to be increased significantly, normal anatomy would make a dangerous amount of plastic explosive with tapered edges difficult if not impossible to detect.

Keywords X-ray imaging · Airport security · Compton backscatter · Explosive detection · Personnel screening

Introduction

Airport whole body scanners are being deployed throughout the US, UK, some airports in continental Europe and other places in the world. The purpose of these

L. Kaufman
University of California, San Francisco, Emeritus, 161 4th Ave, San Francisco, CA 94118, USA
e-mail: kleon01@arnet.com.ar

J. W. Carlson (✉)
Formerly University of California, San Francisco, 240 Cambridge Drive, Kensington, CA 94708, USA
e-mail: joseph.w.carlson@gmail.com

units is to find contraband hidden under clothing but on the surface of the traveler. One of the technologies in use involve x-ray scanning with backscatter imaging.

Referring to Figure 1, in conventional radiography an object of interest (M) which may include an added absorber (A) is placed between a source of x-rays S and an imaging detector I. The detector produces a "negative" of the absorbing power of the M-A combination. X-rays can scatter in M and A and reach the detector, degrading image quality. A grid can be placed between M and I to reduce scatter. In backscatter imaging, a source/collimator (S/C) assembly is scanned over the object of interest, and a non-imaging detector (N-I) is placed between the collimator and the object. X-rays that undergo Compton scatter in the object may reach the detector. Position information is obtained by knowing where the x-ray beam is. Photons can undergo

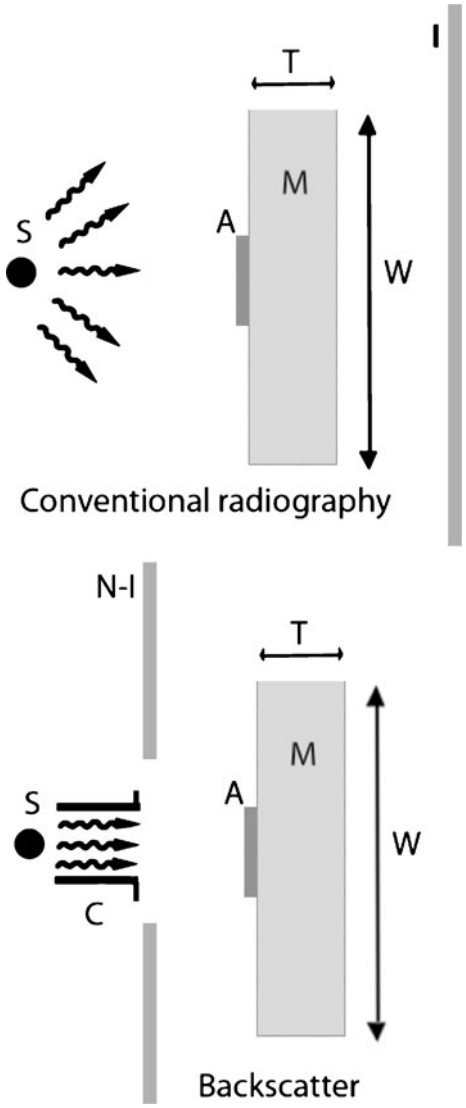

Figure 1 Schematic comparing conventional and backscatter x-ray imaging

scatter anywhere along the beam as they penetrate, and many may scatter a second time and reach the detector, but independently of their origin in the object, are assigned to the beam position. If the beam scans in a pattern parallel to itself, then the x,y (in plane) position is well known but no z (depth) information is known. A corollary is that for a non-parallel beam there will also be small x,y errors due to parallax. There are also hard edge effects as we shall see below.

Compton scatter is a well understood and characterized effect (Evans 1955). The scattered x-ray loses energy in the process, and for 30 and 60 keV x-rays, typical of the values of interest here, and a scattering angle of 145, the once-scattered x-rays have an energy of 27 and 49 keV, respectively. The crossection for the process is given by the Klein-Nishina formula (Evans 1955) and is nearly isotropic at these low energies.

The justification for the safety of these machines rests on two assertions. The first assertion is that the radiation used does not penetrate beyond the skin (for references on this subject see (Kaufman 2010)), second, that the effective dose is no more than 0.1 (or variously 0.05, 0.03, 0.02 or 0.01) microSv (National Council on Radiation Protection and Measurements 2003a, 2003b).

As we discuss below, at the kilovoltage (kVp) setting of the units in use, 50 kVp and 125 kVp, penetration is a given since these are diagnostic x-ray unit settings, and diagnosis depends on penetration through a subject.

Regarding dose, except for the numbers mentioned above, little information exists. The dose from these units is usually referred to what is commonly known as SC 01-16 (National Council on Radiation Protection and Measurements 2003a), which on this subject is a summary of SC 01-12 (National Council on Radiation Protection and Measurements 2003b), with both documents referring to ANSI/HPS Standard N43.17 (Radiation Safety for Personnel Security Screening Systems Using X-ray or Gamma Radiation, ANSI/HPS Draft Standard N43.17). In all cases these are documents that describe the rationale for acceptable exposure levels and discuss methods for measuring “effective dose” in a variety of security devices. The calculation of dose in Sieverts (Sv) is based on an involved use of tables and charts and on assumptions about volumes and organs being exposed-thus the importance of penetration. They also include some allowances for kVp setting. Raw data and the assumptions and recipes by which “effective dose” was calculated for these units are not presented.

To distinguish our results from the published doses, we use the term exposure and we give it in terms of nanogray (nGy) so that it is clear that this is a physical parameter clearly defined and not adjusted for estimates of penetration, the kilovoltage used in the device, and other factors. The “effective dose” published includes factors for the kilovoltage of the unit being tested, and, for instance, is different for front and back exposure, and may be three or six times smaller than the exposure based on energy deposited and the quality factor, which is 1 for x-rays.

Knowledge of the generator and x-ray tube used, kVp setting and filtration. location with respect to collimation, collimator crossection and length, and scanning area and speed, information of little use to a someone intent on passing contraband, as we shall see below-, would permit an accurate evaluation of dose. Of these, kVp settings and filtration, scanning area and scan speed are known from various documents, including (National Council on Radiation Protection and Measurements 2003a, 2003b) and TSA operational requirements (Operational Requirements Documents 2006). Lacking the other parameters, a direct calculation is not possible.

In this paper we show how an understanding of the performance parameters of the backscatter units can be obtained from what has been disclosed together with an analysis of the published images.

Another factor to be considered is sensitivity to contraband. Two views of the subject are presently obtained, one from the front and another from the back. The available images show hard-edged low atomic number Z objects such as water-filled bottles or "bricks" of explosive, and iron in the form of knives or guns. The low Z objects are sometimes peripheral to the body, where the distortion of normal anatomy is clear, and the high Z materials are always presented against the body as a background.

An important factor is safety, what the exposure levels mean in terms of hazards to exposed humans. This is a complex matter, since it needs to take into account dose to each organ, the skin, thyroid, fetus, etc. each responding differently, and the predisposition, genetic or disease-induced, of the exposed individual. The authors have no expertise in the field of the biologic effects of radiation, and we do not enter into the debate as to whether the levels calculated are "safe" or not, or on risk/benefit considerations. As a consequence, we present exposure levels in terms of energy absorbed by a gram of tissue, using the definition of the gray as 10,000 erg/gram for radiation with a quality factor of 1 (which is the case for x-rays and electrons). Exposure levels are given as a function of depth in the tissue, this not being directly comparable to "effective dose" in Sv presented in the published documents.

Input parameters

The x-ray spectra are known from Refs. (National Council on Radiation Protection and Measurements 2003a, 2003b) and others, and are shown in Figure 2 for the two commercial units in use. The higher kilovoltage unit operates at 125 kVp with 1.5 mm Aluminum filtration, and the lower kilovoltage unity at 50 kVp with 1 mm of Aluminum filtration. The first is CT kilovoltage, the second is higher than that used in

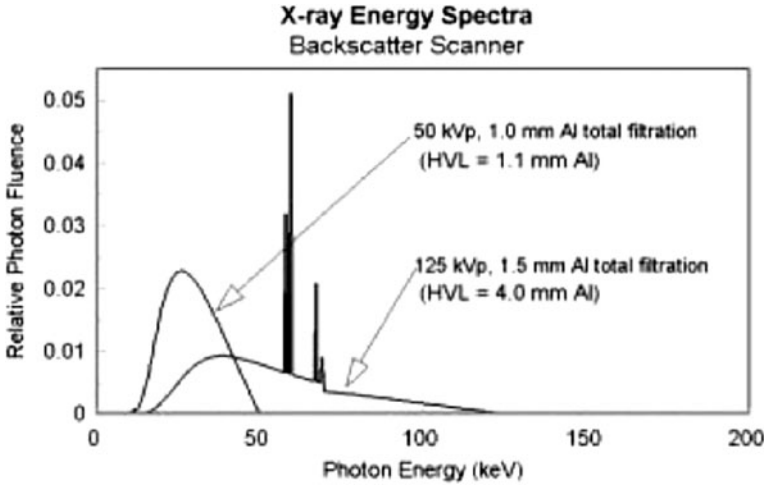

Figure 2 Published x-ray spectra for low and high kilovoltage units, from Refs. (National Council on Radiation Protection and Measurements 2003a, 2003b)

mammography. We will refer to these as high and low kilovoltage units. For calculational purposes, the energy distribution of the beam was approximated by discrete steps (nine steps between 11 and 48 keV for low kilovoltage and 12 steps between 17 and 116 keV for high kilovoltage, so that the K-lines of tungsten are well represented). The beam is assumed to be a pencil beam with no penumbra. As we will see below, the beam dimensions affect spatial resolution but not exposure levels. No knowledge of the beam fluence is needed in this analysis.

The solid angle for the detectors can be reasonably deduced from photos and floor plans available on the web from the manufacturer of the Rapiscan 1000 (low kilovoltage). In our estimates the subject is placed so that, for a 25 cm-thick subject, the front is 26 cm from the front panel of the device (z direction). The detectors are assumed to be in side panels, against their front, and to be 176 cm in the vertical dimension (y), symmetrically placed, and extend from−55 cm to−29 cm and from +29 cm to +55 cm in the horizontal axis (x). The detectors are assumed to be NaI(Tl) with 100% detection efficiency for any photon that reaches their front. The images used in our analysis are shown in Figures 3 and 4.

Rationale

Although the available images are obtained from websites, and consequently can be degraded, the necessary information can be obtained from them, and checked for consistency among various sources.

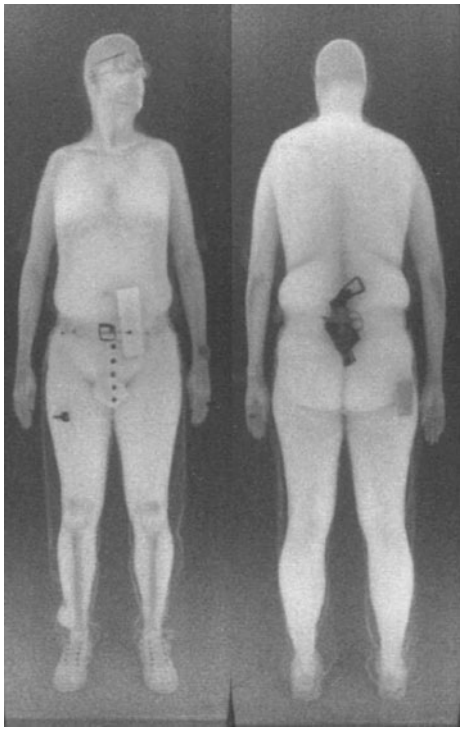

Figure 3 Backscatter image at low kilovoltage. Pixel dimension is 2.1 mm

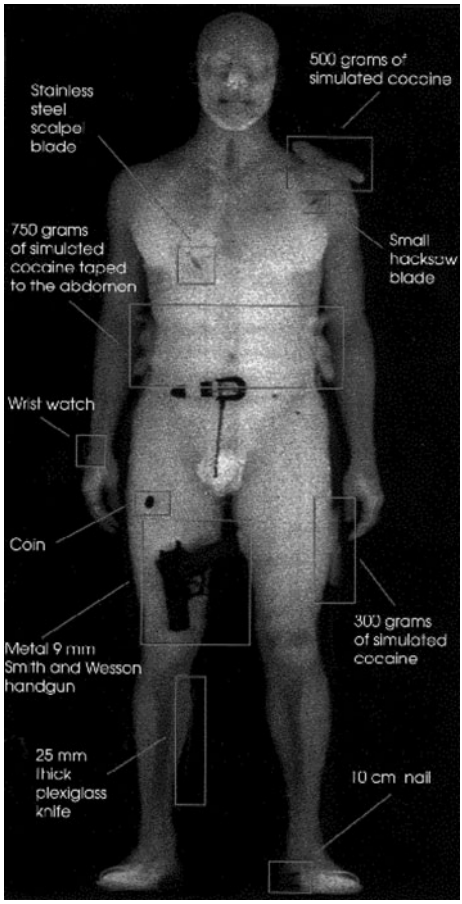

Figure 4 High kilovoltage image apparently unprocessed except for background clipping. The annotations are by the manufacturer

If we know the standard deviation of the counts in pixels in a uniform region of the subject, then, on the reasonable assumption of Poisson statistics, we know how many counts are needed to obtain the measured standard deviation. This is on the assumption that the image has not been smoothed or sharpened or similarly processed. In such a case, an approximate estimate can be obtained by measuring an edge spread function and thus estimating a smoothing function and correcting for it.

To measure standard deviation, small and uniform regions of images were evaluated by recording the intensity value of each pixel in an area of interest and the standard deviation (s.d.) calculated from these values. The signal to noise ratio (S/N) is the mean of the counts in the region divided by the s.d. This ratio can be distorted by non-linearity and by background clipping of data, thus, we examined the images' background (air spaces) to assure ourselves that any clipping present was minimal.

Together with the counts in a pixel we need to know its dimensions, so that we can obtain the counts per cm^2. Note that if the beam is larger or smaller than

the pixel, in so far as the pixel dimension itself is known, the counts are representative of the exposure in that area as the beam scans the subject. The counts/cm^2 are simply given by (10/pixel dimension in mm)^2. The dimension is obtained in our case by (1,760 mm/number of pixels in the y direction). The 1.76 m height is consistent within less than 5% with published cabinet size, with the height for a human, and with government requirements as in Ref. (Operational Requirements Documents 2006).

Image characterization

Figure 3 is a low kilovoltage image. It measures 190±15.3 units in uniform regions, leading to a S/N ratio of 12 on a per image pixel basis. The vertical dimension is spanned by 835 pixels, yielding a pixel dimension of 2.1 mm. This necessitates approximately 144 counts from each pixel, translating to 3,270 counts/cm^2.

Figure 4 shows a high kilovoltage image likely without spatial processing. This image, smoothed, is widely distributed. The y extent is 696 pixels and the pixel dimension 2.5 mm. The image does not appear to have a solid angle correction. The edge transitions are sharp, which are enhanced by clipping. The background in this image is clearly clipped, we estimate that by about 14 units. We measure, in a bright and uniform region 145±21 units, this resulting in a S/N of 7. Assuming 14 units of clipping the S/N is approximately 8. This necessitates from 49 to 64 counts in a pixel, translating to 784 to 1,024 counts/cm^2.

Using Figure 4 as a reference, our exposure calculations will be referenced to 55 counts per 2.5 mm pixel. We will also show some results over a range of count/pixel and pixel dimension values. The conversion is simple: Exposure increases linearly with the number of counts per pixel and it decreases with the square of the pixel dimension. Exposure increases as the square of the S/N in a pixel.

Methods

The geant4 (Agostinelli et al. 2003) Monte Carlo program was run with the geometry as described above. In as much as possible, existing geant4 models were used as the basis of the simulation software. In particular, the human phantom model of Guatelli et al. (Guatelli et al. 2006) was used for the constituent model of soft tissue and the physics components (low energy Rayleigh scattering, photoelectric effect, Compton scattering and gamma conversion) were included in the simulation. The general suitability of geant4 for modeling low energy x-ray processed has been described elsewhere (Fiejo and Hoff 2008). Initially, the performance of the program and data extraction were studied at a beam energy of 60 keV, close to the average energy of the high kilovoltage unit. The data presented here were for high and low kilovoltage spectra as described above. The beam had a 2.75 mm×2.75 mm dimension. We note again that beam dimension does not affect exposure. The runs consisted of 50,000 incoming x-rays at high and low kilovoltage, for the calculation of exposure and penetration. We found that to be able to make reasonable statements about sensitivity to explosives we needed much higher statistics, and made runs of

2.5 million x-rays at low kilovoltage and 1 million x-rays at high kilovoltage for the calculation of sensitivity.

We performed six simulations at each kilovoltage.

Simulation 1: An x-ray beam impinging the center of a block of tissue of dimensions 40 cm×40 cm (W in Figure 1) and thickness along the beam direction of 25 cm (T in Figure 1).

Simulation 2: The block of Simulation 1 with an added block of tissue (A in Figure 1) centrally located and 20 cm×20 cm dimension, 1 cm thickness. Except for a minor solid angle change due to being 1 cm closer to the detector, the results of Simulations 1 and 2 should be the same.

Simulation 3: Same as Simulation 2, but the added block (A in Figure 1) simulates TATP explosive, or triacetone triperoxide, with density 1.19 and composition C9H18O6.

Simulation 4: Same as Simulation 3 but with a density of 1.2. The slightly different density was intended for checking consistency of results.

Simulation 5: Same as Simulation 2, but the added block (A in Figure 1) simulates PETN explosive, or pentaerythritol tetranitrate, with density 1.8 and composition C5H8N4O12.

Simulation 6: Same as Simulation 5 but with a density of 2.0. The slightly different density was intended for checking consistency of results.

The six runs will be referred to as Den0, Den1,...Den6, respectively followed by Low or High for the kVp setting.

The values extracted for this paper are: A. Energy deposition in eV in the target in 1 cm-thickness steps for an area of 1 cm×1 cm, so that approximating the tissue density by 1, the exposure in Gy is easily scaled from the energy deposited. B. The percent of events detected as a function of their depth of origin in tissue. C. The x,y origin in tissue of the detected events. D. The sensitivity to explosives under various exposure values.

In addition we performed imaging simulations of various objects.

Results

Penetration and exposure

Figure 5 shows the exposure in nanoGy to obtain 55 counts per 2.5 mm×2.5 mm pixel for the high and low kilovoltage units, using only tissue in the Den0 (subject surface at 26 cm from the detectors) and Den1 (subject surface at 25 cm from the detectors) configurations. In the figure, the first cm of tissue encountered by the beam is listed as a depth of 0 cm. For equal counts, the low kilovoltage unit delivers a four times higher entrance exposure, the exposures becoming equal at about 7 cm of depth. Figure 6 shows the same data summed to simulate exposure after two views (the normal usage mode) of a 25 cm tissue thickness. It can be seen that for the high kilovoltage case the exposure around the center drops to about 60% of the surface exposure and is higher than that of the low kilovoltage unit. For a given

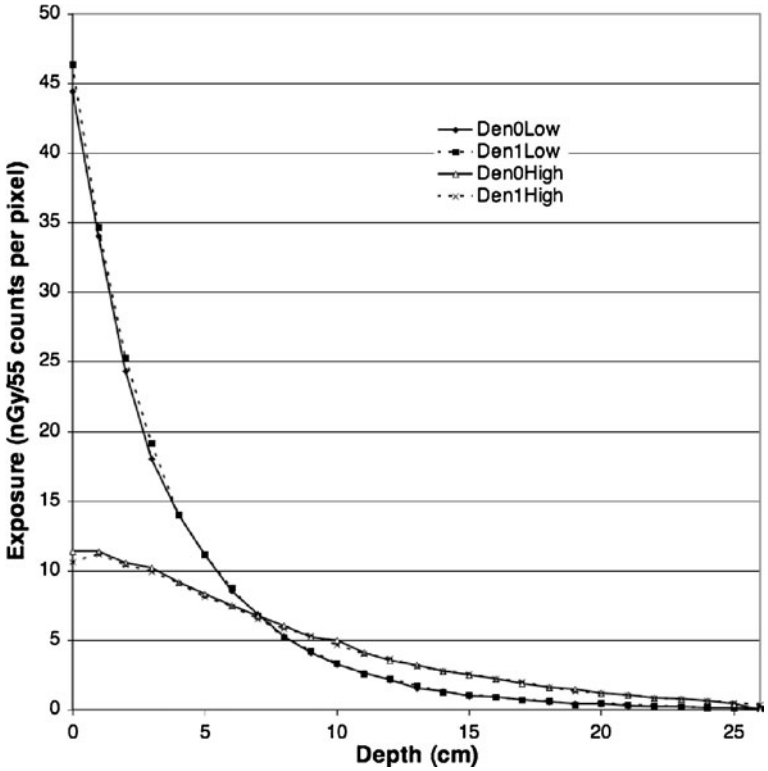

Figure 5 Exposure in nGy for tissue at high and low kilovoltage. The exposure is referenced to 55 counts per pixel and a 2.5×2.5 mm^2 pixel dimension

number of counts, the average exposure through the 25 cm of tissue is 1.6 times higher for the low kilovoltage unit. Thus, at 50 kVp, equal statistics require higher entrance and average exposure than at 125 kVp. We note that fewer than 2% of the photons in the low kilovoltage x-ray beam scatter into the detector, and that for high kilovoltage less than 5% do. The detection efficiency as a function of incoming x-ray energy is shown in Figure 7.

As would be expected, very little of the beam scatters from the skin or even a 1 cm below it. Figure 8 shows the deepest point in the tissue from which events reach the detector. At low kilovoltage less than half the image counts come from the first cm of the subject, a significant amount come from within 5 cm of depth, and some as deep as 15 cm. At high kilovoltage, less than a quarter come from the first cm, a significant fraction come from the first 10 cm, and some from as deep as 20 cm. We note also that events assigned to the pixel on which the beam rests also come from scattering at remote x,y locations in the tissue (Figure 9 (high kilovoltage) and 10 (low kilovoltage)), as many as 30% from farther than a cm from beam center at high kilovoltage (Figure 9).

Beam penetration into tissue decreases the sensitivity to higher density explosives. Consider that half of the events arise from below a cm of depth. A 1 cm layer of low atomic number (Z) material, such as explosives with average Z of near 7, not that different from tissue, will stop more incoming x-rays and increase

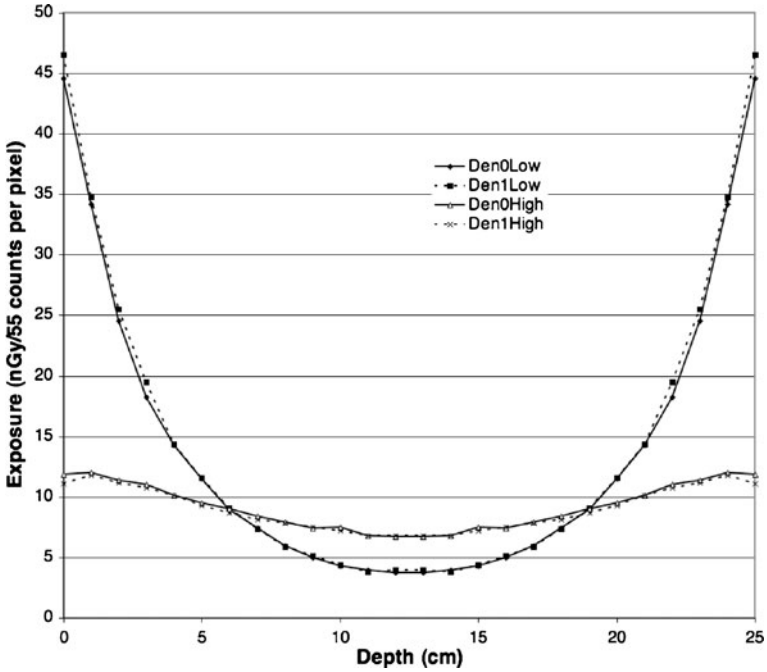

Figure 6 Same data as in Figure 5 but summed so as to simulate the exposure of a 25 cm thickness of tissue

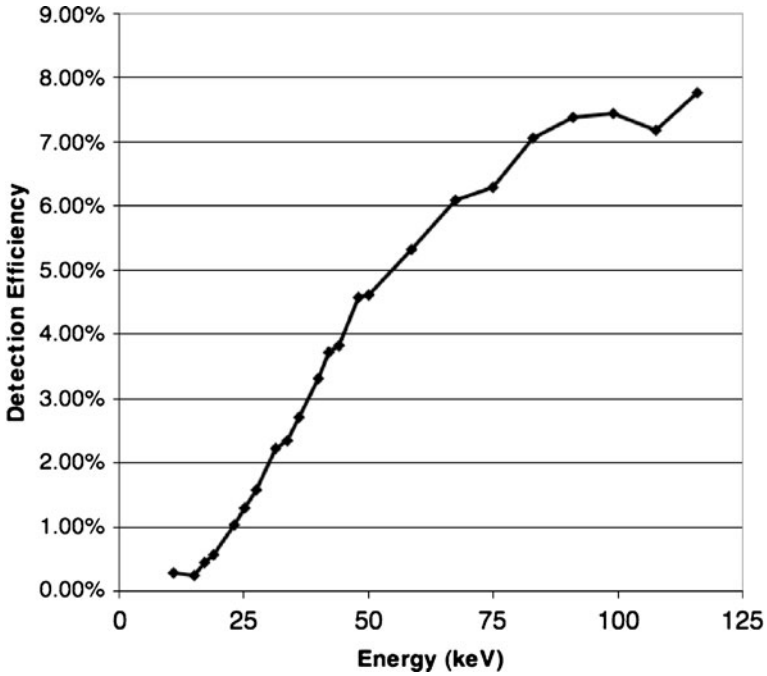

Figure 7 Efficiency, defined as the number of counts recorded by the detectors as a fraction of the number of x-ray inputs, shown as a function of input x-ray energy

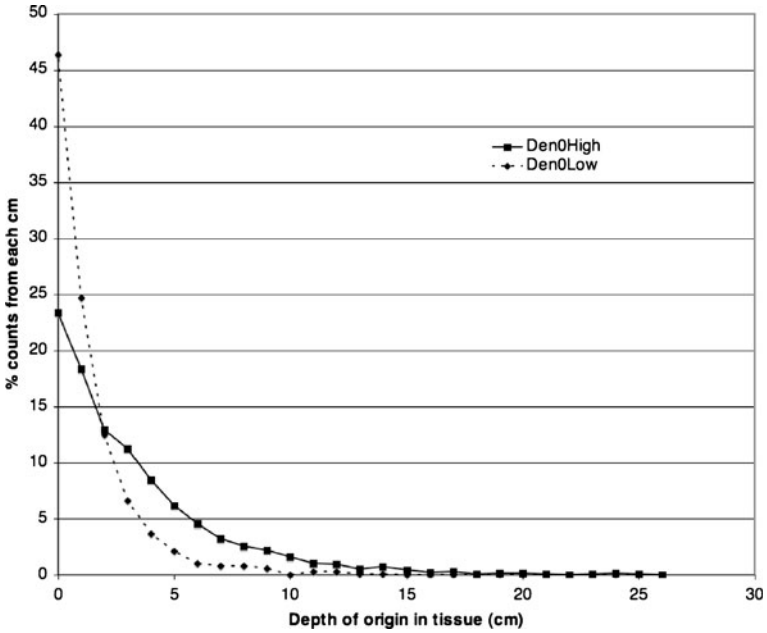

Figure 8 Deepest point of interaction in tissue of x-rays that form the backscatter image

scatter per cm of depth, but will also decrease the number of x-rays reaching deeper into tissue and the backscattered photons from deep in, so that effects in the explosive layer and in tissue will be in opposite directions, reducing sensitivity. Penetration also provides an obvious explanation for air-space shadows such as lung

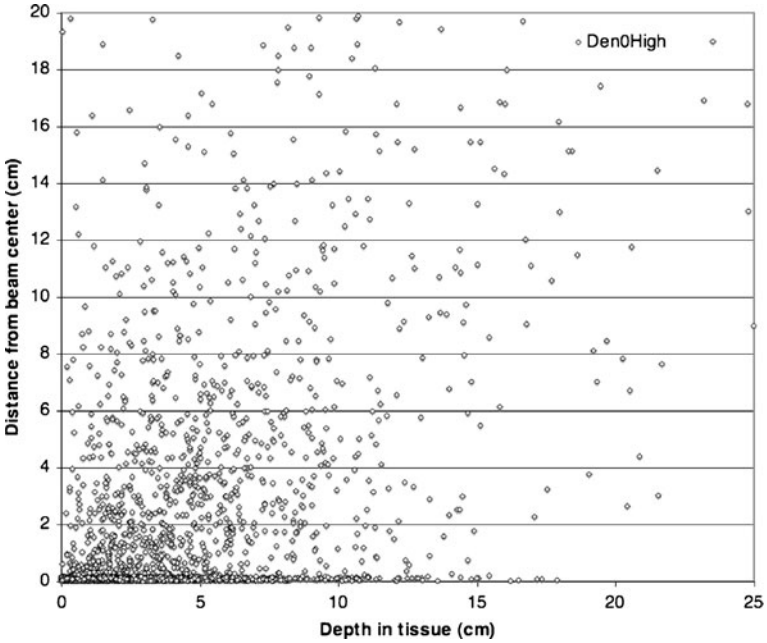

Figure 9 Distance in tissue from beam center where x-rays forming the image have an interaction, high kilovoltage

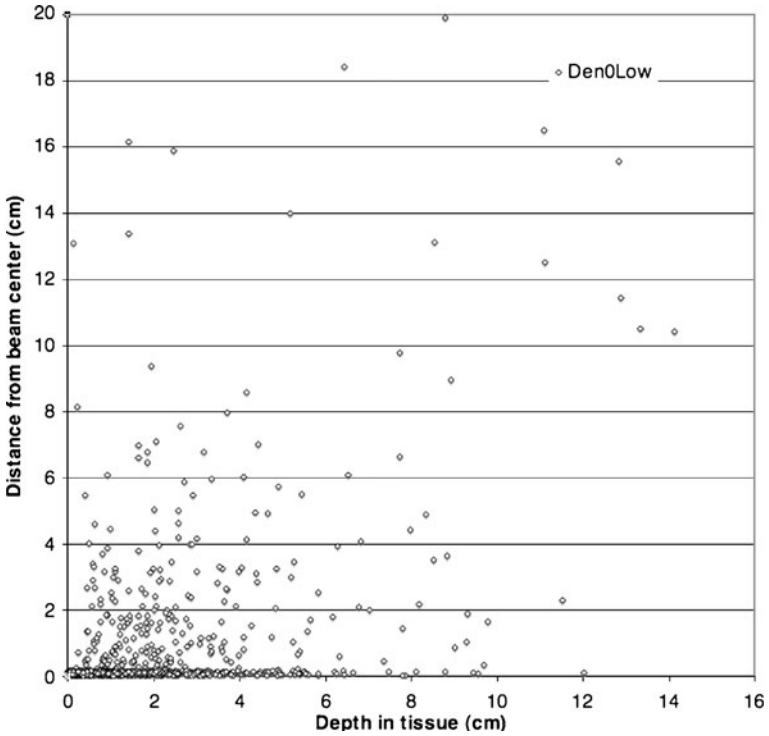

Figure 10 Distance in tissue from beam center where x-rays forming the image have an interaction, low kilovoltage

shadows. Consider 2 cm of tissue of density 1 followed by lung of density 0.3. At high kilovoltage, the first 2 cm of depth contribute the same roughly 42% of events, but the other 58% are reduced by a factor of 0.3, so that the image contains 60% as many counts over lung than over solid tissue, the value that we measured in high kilovoltage units. At low kilovoltage the effect is less pronounced, and the images show less conspicuous air spaces.

High density, high Z materials will scatter very few x-rays and when in front of tissue will appear dark but with some background counts at high kilovoltage (about 3.5% of tissue signal).

Sensitivity

Figures 11 and 12 show the sensitivity to explosives. Figure 11 has error bars that correspond to the statistics of the Monte Carlo calculation (approximately 50,000 detected events for each kilovoltage scaled to 55 counts at Den0). Figure 12 shows the error bars corresponding to 55 counts. The statistics of the Monte Carlo calculation (s.d.≈0.45%) exceed the excursion of the different materials tested. The Den0 and Den1 tissue only runs are within 1 s.d., as are the Den3 and Den4 pair (TATP, differing in density by less than 1%) and Den5 and Den6 runs (PETN, differing in density by 10%) are closely matched, raising confidence in the statistics of the calculation. The excursion for TATP amounts to approximately 8% at low

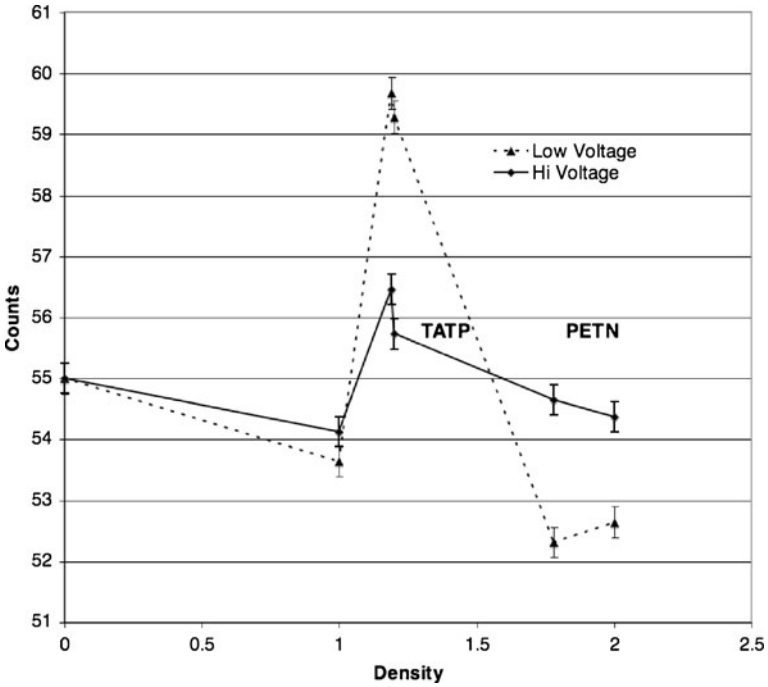

Figure 11 Counts per pixel for the different configurations evaluated. Tissue alone at 26 cm from the detector plane is at the zero density point. At the density 1 point a cm of tissue is added to the tissue front. TATP with densities 1.19 and 1.2, and PETN with density 1.78 and 2.0 are added to the configuration of zero density. The statistics are those of the Monte Carlo calculation

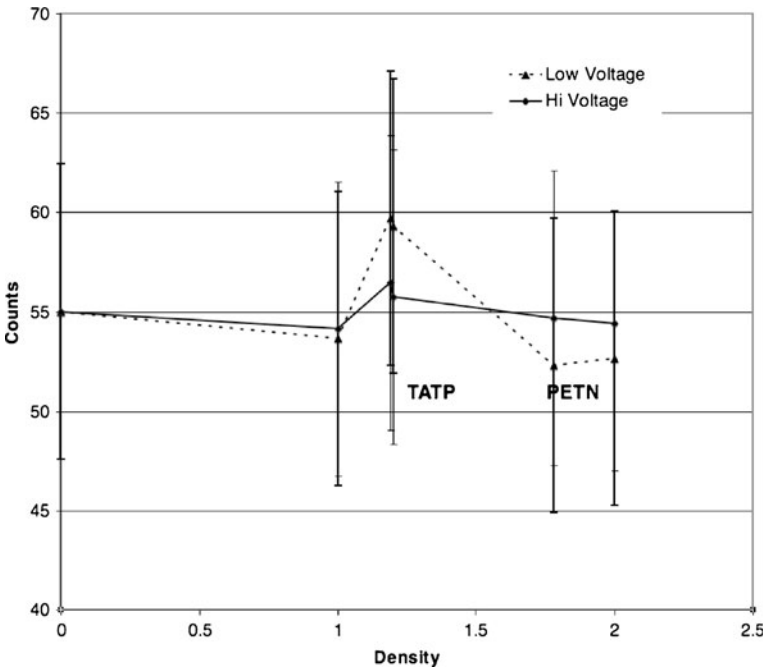

Figure 12 Same as Figure 11 with Poisson statistics of 55 counts

kilovoltage and it is −4.5% for PETN. The excursions for the two explosives at high kilovoltage are 1.6% for TATP and −1% for PETN.

Table 1 shows standard deviations in percents under different conditions. Recalling that the reference conditions are 55 counts per 2.5 mm×2.5 mm pixel, Table 1 shows the s.d. for an entrance exposure of 100 nanoGy (the ANSI standard and current limit for these devices is 0.1 microSv "effective dose") and a pixel of 6 mm×6 mm. The s.d. at low kilovoltage is twice as large as that at high kilovoltage, e.g., for fixed exposure and spatial resolution the low kilovoltage images are grainier, but its signal excursion, or difference from no added object, for TATP is four to five times larger. The excursions are about half as large for PETN, a similar factor is calculated between the two voltages.

For S/N value of 12 and 20, to keep entrance dose below 100 nanoGy, pixel area has to be larger than 6 and 20 mm^2 at high and low kilovoltage, respectively (Figure 13).

There exists some room for lowering of exposure results by a change in the input parameters used. The detector efficiency is assumed at 100%, even though for the kind of technology in use in this market, heavily influenced by number of units and budget, and little influenced by competitiveness and performance, the efficiency may easily be 50%. Thus, the 100% efficiency used here is a generous estimate. The detector outside dimensions are limited by cabinet dimensions. It is possible to increase detection solid angle by narrowing of the inside distance between detectors, thereby increasing the horizontal angular variance of the x-ray beam, and such narrowing is included in the imaging simulations.

Smoothing increases S/N with consequent penalty on spatial resolution. Figure 14 shows the same data as that of Figure 4, but processed with smoothing and edge enhancement, as evidenced by overshoots at sharp edges. There are 825 pixels in the y direction, making pixel size 2.1 mm. Edge spread is 6 to 7 pixels, making the spatial resolution in the image 12 to 14 mm. This image is the version of the image of Figure 4 that is widely available on published documents.

Based on these results, some conclusions can be reached on the detectability of explosives. Considering TATP, at low kilovoltage, in the configuration evaluated here, the signal is 8.1% higher than that measured in its absence. The noise for a 2.5 mm square pixel is 13.5% at an entrance exposure of 45 nGy (Table 1, Figure 5). Following Rose (Rose 1971), the detectability of a change in signal for a pixel is measured as Signal Difference (SD)/noise (N) and needs to be in the range of 4. For Poisson statistics, this is equivalent to stating that reliable detection depends on the SD being four times larger the s.d. In this case, for 8.1% SD, the noise should be at

Table 1 Sensitivity examples.

Signal excursion (%)	Monte Carlo s.d. (%)	s.d. at 55 counts, 2.5 mm pixel (%)	s.d. at 100 nGy entrance exposure, 6 mm pixel (%)
Low kVp			
8.1 (TATP) 4.6 (PETN)	.45	13.5	7.2
High kVp			
2.0 (TATP) 0.9 (PETN)	.45	13.5	3.7

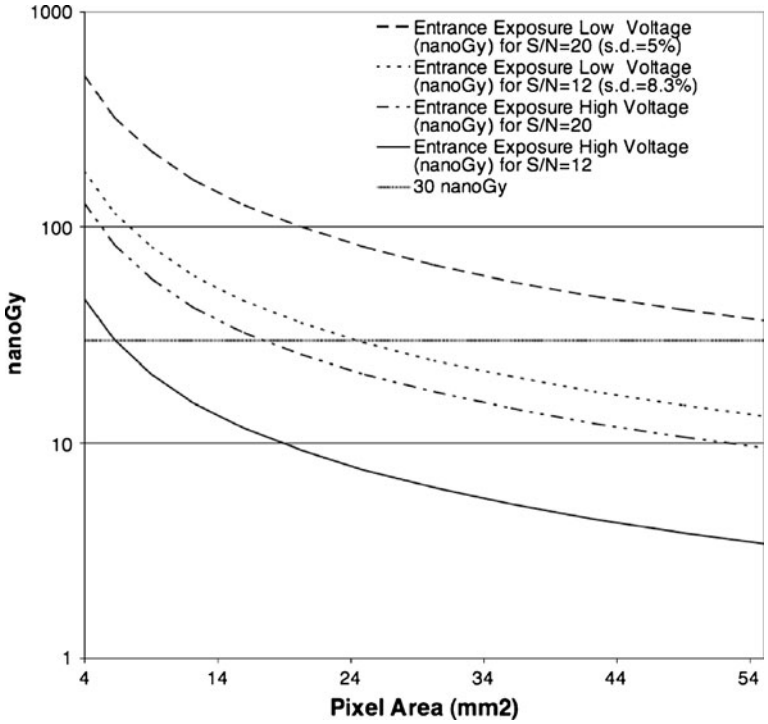

Figure 13 Scaling of entrance exposure at high and low kilovoltage. The range of 10–30 nGy (in Sv units) is widely quoted as the "effective dose" of the backscatter units (National Council on Radiation Protection and Measurements 2003a, 2003b), while the shown values are entrance exposures

2% at the single pixel level. Given the 1 pixel-scale noise of 13.5%, this requires 46 times more counts, and concomitant exposure. To reach Rose's criterion the entrance exposure would need to be 2,070 nGy for a 2.5 mm pixel, or the pixel dimension 17 mm for the exposure of 45 nGy. At an entrance exposure of 100 nGy the pixel dimension would need to be 11 mm.

Similarly, for TAPT at high kilovoltage, the SD is 2.0%, the 1 pixel level noise is 13.5% at an entrance exposure level of 1.14 nGy. To meet Rose's criterion the noise should be 0.5%, this necessitating 730 times more counts and exposure, leading to an entrance exposure of 8,320 nGy for a 2.5 mm pixel, or a pixel dimension of 68 mm at an entrance exposure of 11.4 nGy. At an entrance exposure of 100 nGy the pixel dimension would need to be 23 mm.

For PETN the conditions are worse. At low kilovoltage the entrance exposure needed to meet Rose's criterion is 6,210 nGy for a 2.5 mm pixel, or the pixel dimension 29 mm for the exposure of 45 nGy. At high kilovoltage the entrance exposure is 41,000 nGy for a 2.5 mm pixel, or the pixel dimension 150 mm for the exposure of 11.4 nGy. At an entrance exposure of 100 nGy the pixel dimensions would need to be 19 mm and 51 mm at low and high kilovoltage, respectively.

It can be argued that the eye is able to average signal over large areas, so that the pixels can be small and yet viewing conditions can be set for optimal averaging. This is true when the noise in the image is stochastic at all spatial frequencies. If there is structure, e.g., variations such as those created by anatomic variability and various

Figure 14 Backscatter image at high kilovoltage. This image (same as Figure 4) has a been smoothed and edge enhanced. Pixel dimension is 2.1 mm

benign objects, as is clearly the case in the images, then the noise at any one spatial frequency is given by the quadratic sum of the stochastic and structured noise (Shosa and Kaufman 1981). Consider Figure 3 with a S/N of 12 on a per 1 pixel basis. If the eye were to average over an area of 10,000 pixels (a diameter of 11 cm), the perceived S/N would be 1,200, sufficient for the task of reliably detecting 1–8% variations. Nevertheless, over the spatial extent of 11 cm, the torso of Figure 3, which is far more featureless than the abdomen, shows a S/N of 5, wholly inadequate to the task, and not improved by reducing stochastic noise.

It is worth noting that Figure 3, with a pixel dimension of 2.1 mm and a S/N of 12, this simulation requires an entrance exposure of 170 nGy, 70% higher than the ANSI guideline.

As we shall see below, these units depend on hard edge effects for the purpose of detection.

Imaging

For demonstration of image characteristics in x-ray backscatter systems, we simulated an abdomen by a cylindrical (45 cm-tall in a 50 cm field of view) uniform tissue elliptical phantom, 45 cm-wide and 25 cm-thick, the closest point of the front placed at a 26 cm distance from the plane of the detector. For imaging, detector dimensions were changed from the above evaluations: While the height and outside dimensions are limited by cabinet sizes, we assumed for imaging a smaller dead space between right and left detector, 18 cm rather than 58 cm. The effect of this change is to increase sensitivity *at the center* by factors of 3.4 and 3.6 at high and low kilovoltage, respectively. Detector performance continued to be assumed at 100% for all photons reaching its surface. The pixel size was 2.5 mm×2.5 mm, and the beam dimension 6 mm×6 mm. The display is for 5 mm×5 mm pixels, with the average of the four pixels forming it.

Four examples were simulated. No added material, added tissue, added TATP at density 1.2 and added PETN at density 2.0. These added materials were configured as a cone or "pancake" of 20 cm-diameter, 1 cm-height at the center, tapering to zero thickness at the border and conformal with the "abdomen". The volume of this added material was approximately 160 cm^3, making the weight of PETN approximately 320 g (note that the "shoe bomber" and "Christmas bomber" were reported to carry 40 g and 80 g of PETN, respectively, both considered sufficient to blow a hole in an aircraft fuselage.)

We compared these images to those of a tissue "brick" of the same volume (15 cm×10 cm, 1 cm-thickness, 150 g), the brick geometry being typically used for demonstrations of backscatter detection capabilities.

All tests included a water bottle of 3 cm-diameter and 5 cm-length, and an iron bar of 10 cm×1 cm and 1 mm-thickness. For all images, the entrance exposure is 10 nanoGy. Counts at this exposure are shown in Table 2. It is important to note that the 10 nanoGy exposure images shown here are a best case assumption. Detector efficiency is likely to be 50% of the value assumed, or even less at low kilovoltage, especially for multiple-scattered photons. The solid angle can be as much as 3.5 times lower, and is certainly less away from center, especially as departing center in the vertical direction, so the exposure could reach 70 nanoGy, close to 100 nGy

Table 2 Imaging results for 10 nGy entrance exposure.

Pixel size (mm × mm)	Counts	s.d. (%)
High kVp, 40,000,000 input x-rays		
2.5×2.5	170	7.7
5×5	680	3.8
10×10	2,720	1.9
Low kVp, 25,000,000 input x-rays		
2.5×2.5	44	15
5×5	176	7.5
10×10	704	3.8

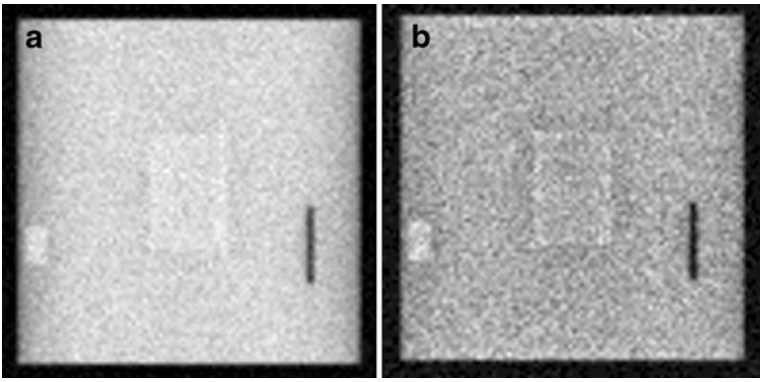

Figure 15 Simulated images at high (**a**) and low (**b**) kilovoltage for 10 nGy entrance exposure of a 150 g brick of tissue (15×10×1 cm). The center intensity is approximately 4.5% higher than background because of edge effects. Note that the brick is of the same composition as the underlying "abdomen". If the brick were larger, its internal signal would be that of surrounding tissue

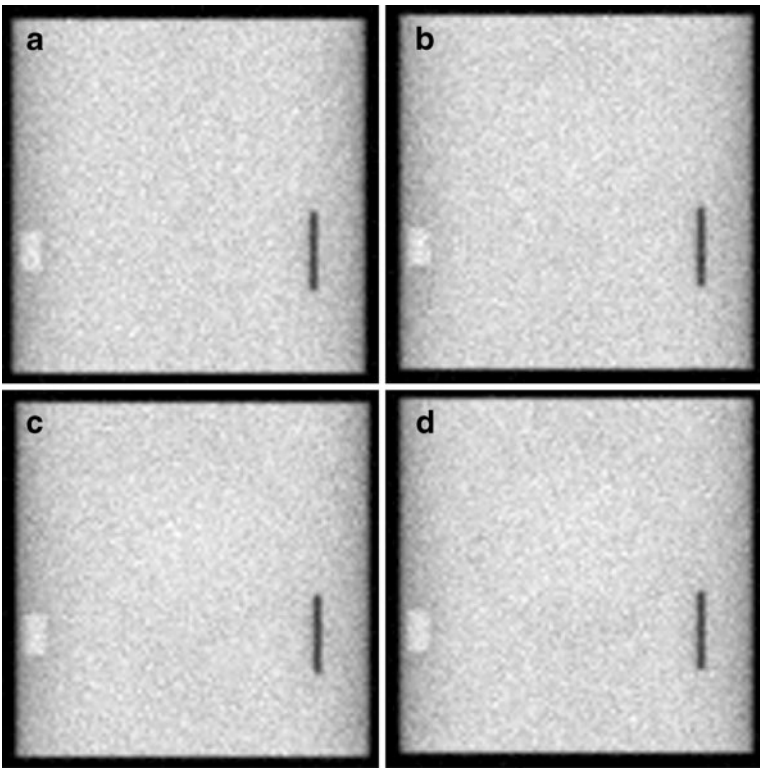

Figure 16 Simulated images at high kilovoltage for 10 nGy entrance exposure. data were acquired in 2.5 mm (200×200 matrix) pixels and are averaged and displayed with 5 mm pixels. **a** Tissue only; **b** Added 1 cm-thick, 20 cm-diameter pancake of 160 g of tissue; **c** Same as B, but with 190 g of TATP (density 1.2); **d** Same as B, but with 320 g of PETN (density 2.0)

A characteristic of backscatter imaging is a hard edge effect akin to a high pass filter with overshoot. Consider an x-ray beam scanning along a flat surface from, say, left to right. Most of the x-rays scattered into the detector come from deep into the subject, many not even from the beam position (Figures 8, 9, and 10), and they leave through the surface. For a uniform surface, neglecting solid angle changes, the scattered intensity is uniform. As the beam approaches a step that makes the material thicker, deep-scattered x-rays have more material to traverse if they scatter right rather than left. At the edge itself, half of the scattered x-rays have to traverse more material to exit, and there is a maximum drop in signal intensity. Consider now the beam scanning along the stepped material from right to left. Except for a small change in solid angle (proximity to detectors), the intensity is uniform and the same as for the beam in the far left. As the beam approaches the edge, some deep-scattered photons now can exit through less material, and the signal intensity increases, reaching a maximum at the edge. Thus, in a scan, there will be an undershoot at the edge on the lower surface, and an overshoot on the higher surface side. This effect will be unidirectional if the detectors are not symmetrical with respect to the edge location.

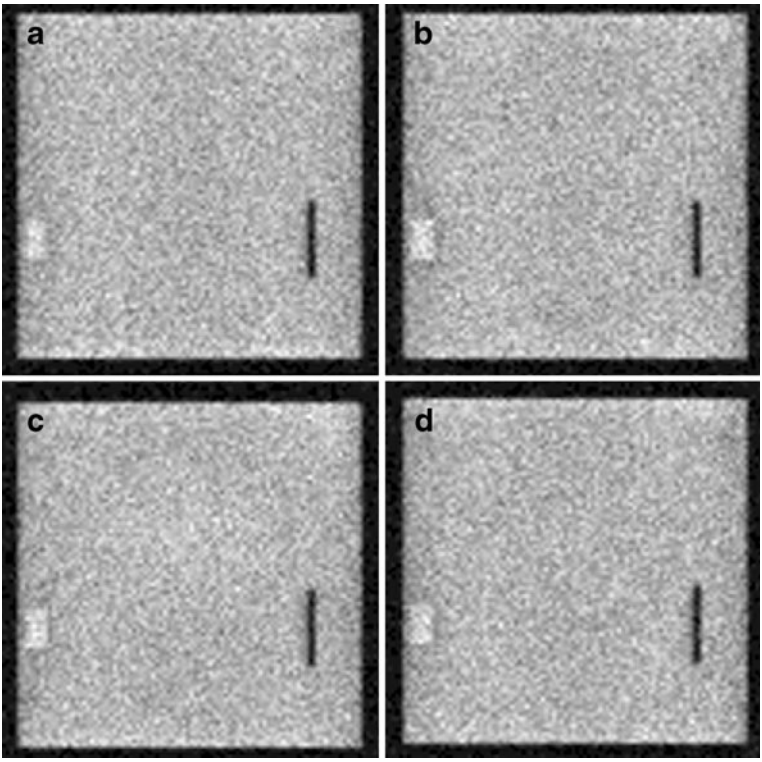

Figure 17 Simulated images at low kilovoltage for 10 nGy entrance exposure. data were acquired in 2.5 mm (200×200 matrix) pixels and are averaged and displayed with 5 mm pixels. **a** Tissue only; **b** Added 1 cm-thick, 20 cm-diameter pancake of 160 g of tissue; **c** Same as B, but with 190 g of TATP (density 1.2); **d** Same as B, but with 320 g of PETN (density 2.0)

Figure 15 shows the tissue brick at high and low kilovoltages. The brick is clearly visible since it is almost all "edge", given the beam spread shown in Figures 9 and 10, and more so at high than at low kilovoltage.

Figure 16 shows the abdominal phantom at high kilovoltage. Figure 16a is for the abdominal phantom with the bottle and iron alone. Figure 16b includes a pancake of tissue, which is not discernible. Figure 16c and d are for TATP and PETN respectively. The TATP shows as a faint increase in signal around its center, and the PETN also exhibits a faint dark ring at its periphery. Given the featureless background and knowledge of where to look, there are indications of the presence of these contraband materials. Figure 17 is for the low kilovoltage case. Again, knowing its presence, the TATP is faintly visible as a signal increase at the center, not that different of what can be an anatomic feature (see Figures 3, 4, 14 and 18).

Discussion

The publicly available information on backscatter airport scanners permits a reasonable evaluation of their performance. The results indicate that the radiation used penetrates throughout the body, a not surprising fact to those familiar with radiologic imaging at 50 and 125 kVp. Empirical support comes from noting that the routine diagnostic use of x-ray CT is practiced at 80 kVp to 120 kVp. Mammography, similarly needing enough x-rays leaving a breast of 10 cm or more thickness to make exquisite resolution and S/N images, is practiced at well below 50 kVp.

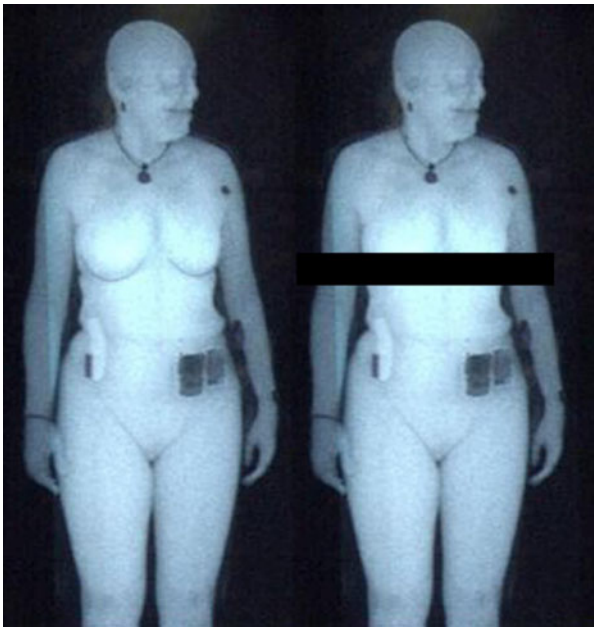

Figure 18 Demonstration of the importance of edge effects to detection. The breast blends into the shading of the image when the lower edge is covered. ?Separately, note that the heavy object on her left hip (a handgun) is only noticeable because her arm allows for a shadow of part of it. Arms raised, as they would have been in normal use, this object would be hard to notice

The penetration not only distributes exposure throughout the body (this affecting the calculation of efective dose, which comprises a sum over all organs), but tends to diffuse the effects caused by contraband materials. Images can be made at low entrance exposures, but of very poor spatial resolution and S/N. The calculated signal excursions at high kilovoltage are so small as to make it doubtful that at any reasonable exposure levels density differences will be noticeable unless the contraband is packed thickly and with hard edges. Although the excursions are larger at low kilovoltage, they are still small and in the noise of the device's operational limits. The eye is a good signal averager at certain spatial frequencies, but it is doubtful that an operator can be trained to detect these differences unless the material is hard-edged, not too large and regular-shaped. Anatomic features and benign objects add structured noise that interferes with signal averaging. Figure 18 shows a widely-distributed backscatter image. On the left is a complete view of her torso, on the right, a section has been blacked out. While the breasts are easily recognized at right, without some prior knowledge of the subject, it would be hard to distinguish the increase of intensity in the superior part of her breasts from the natural gradients of the image.

It is very likely that a large (15–20 cm in diameter), irregularly-shaped, cm-thick pancake with beveled edges, taped to the abdomen, would be invisible to this technology, ironically, because of its large volume, since it is easily confused with normal anatomy. Thus, a third of a kilo of PETN, easily picked up in a competent pat down, would be missed by backscatter "high technology". Forty grams of PETN, a purportedly dangerous amount, would fit in a 1.25 mm-thick pancake of the dimensions simulated here and be virtually invisible. Packed in a compact mode, say, a 1 cm×4 cm×5 cm brick, it would be detected.

The images are very sensitive to the presence of large pieces of high Z material, e.g., iron, but unless the spatial resolution is good, thin wires will be missed because of partial volume effects. It is also easy to see that an object such as a wire or a box-cutter blade, taped to the side of the body, or even a small gun in the same location, will be invisible. While there are technical means to mildly increase the conspicuity of a thick object in air, they are ineffective for thin objects such as blades when they are aligned close to the beam direction.

Acknowledgement The authors are grateful for the valuable input provided by Professor Peter Rez of the Physics Department, Arizona State University.

References

Agostinelli S, Allison J, Amako K et al (2003) Geant4—a simulation toolkit. Nuclear instruments and methods in physics research section A: Accelerators, Spectrometers, Detectors and Associated Equipment 506(3):250–303. (http://geant4.cern.ch/)

Evans RD (1955) The atomic nucleus. McGraw-Hill Book Co., New York

Fiejo PV, Hoff G (2008) Geant4 validation on mammography applications. Nuclear Science Symposium Conference Record IEEE 3497–3498

Guatelli S, Mascialino B, Pia MG, Pokorski W (2006) Geant4 anthropomorphic pantoms. Nuclear Science Symposium Conference Record IEEE 1359–1362

Kaufman L (2010) Letter to the Editor. Re: airport full body scanners. JACR 7(8):655

National Council on Radiation Protection and Measurements (2003a) Commentary No 16- Screening of humans for security purposes using ionizing radiation scanning systems. Bethesda, MD

National Council on Radiation Protection and Measurements (2003b) President report on radiation protection advice: screening of humans for security purposes using ionizing radiation scanning systems (SC 01-12,), Bethesda, MD

Operational Requirements Document (2006) Whole body imager aviation applications, USDHS, July, Version 1.9, Final Report. NTIS, Springfield, VA

Rose AA (1971) Vision: human and electronic, Chapter 1. Plenum, New York

Shosa DW, Kaufman L (1981) Methodology for evaluation of diagnostic imaging instrumentation. Phys Med Biol 26:101–112